A Comparison of Antarctic Ice Sheet Surface Mass Balance from Atmospheric Climate Models and In Situ Observations

Yetang Wang,[a] Minghu Ding,[b] J. M. van Wessem,[c] E. Schlosser,[d,e] S. Altnau,[d,f]
Michiel R. van den Broeke,[c] Jan T. M. Lenaerts,[c] Elizabeth R. Thomas,[g]
Elisabeth Isaksson,[h] Jianhui Wang,[i] Weijun Sun[a]

[a] College of Geography and Environment, Shandong Normal University, Jinan, China
[b] Institute of Climate System, Chinese Academy of Meteorological Sciences, Beijing, China
[c] Institute for Marine and Atmospheric Research Utrecht, Utrecht University, Utrecht, Netherlands
[d] Institute of Atmospheric and Cryospheric Sciences, University of Innsbruck, Innsbruck, Austria
[e] Austrian Polar Research Institute, Vienna, Austria
[f] German Weather Service, Offenbach, Germany
[g] British Antarctic Survey, Cambridge, United Kingdom
[h] Norwegian Polar Institute, Fram Centre, Tromsø, Norway
[i] Department of Pathology, Yale University, New Haven

ABSTRACT

In this study, 3265 multiyear averaged in situ observations and 29 observational records at annual time scale are used to examine the performance of recent reanalysis and regional atmospheric climate model products [ERA-Interim, JRA-55, MERRA, the Polar version of MM5 (PMM5), RACMO2.1, and RACMO2.3] for their spatial and interannual variability of Antarctic surface mass balance (SMB), respectively. Simulated precipitation seasonality is also evaluated using three in situ observations and model intercomparison. All products qualitatively capture the macroscale spatial variability of observed SMB, but it is not possible to rank their relative performance because of the sparse observations at coastal regions with an elevation range from 200 to 1000 m. In terms of the absolute amount of observed snow accumulation in interior Antarctica, RACMO2.3 fits best, while the other models either underestimate (JRA-55, MERRA, ERA-Interim, and RACMO2.1) or overestimate (PMM5) the accumulation. Despite underestimated precipitation by the three reanalyses and RACMO2.1, this feature is clearly improved in JRA-55. However, because of changes in the observing system, especially the dramatically increased satellite observations for data assimilation, JRA-55 presents a marked jump in snow accumulation around 1979 and a large increase after the late 1990s. Although precipitation seasonality over the whole ice sheet is common for all products, ERA-Interim provides an unrealistic estimate of precipitation seasonality on the East Antarctic plateau, with high precipitation strongly peaking in summer. ERA-Interim shows a significant correlation with interannual variability of observed snow accumulation measurements at 28 of 29 locations, whereas fewer than 20 site observations significantly correlate with simulations by the other models. This suggests that ERA-Interim exhibits the highest performance of interannual variability in the observed precipitation.

1. Introduction

Snow falling each year on the Antarctic Ice Sheet is equivalent to 6 mm of global mean sea level (Church et al. 2001). Giant ice in the Antarctic Ice Sheet has the potential to raise global sea level by about 58.3 m if it all melted (IPCC 2013), indicating that even minor changes in its volume will have significant impacts on atmospheric circulation, the global hydrological cycle, sea surface temperature, seawater salinity, and the thermohaline circulation. Therefore, an accurate quantification of Antarctic mass balance is pivotal for detecting the current state of the ice sheet, predicting its potential contribution to sea level, and for understanding the global climate and hydrological cycle. However, the magnitude and sign of Antarctic ice sheet mass balance has long been unclear (Bentley 1993), due to the inherent

Corresponding author address: Yetang Wang, Shandong Normal University, College of Geography and Environment, Wenhua Dong Road 88, Jinan 250014, China.
E-mail: wangyetang@163.com

uncertainties of the methods including observed surface elevation, satellite gravimetry, and the input–output method, that is, quantifying the difference between ice discharge and surface mass balance (SMB). Although there has been increasing evidence of a negative Antarctic mass balance in the past decades (Allison et al. 2009; Chen et al. 2009; Shepherd et al. 2012; Velicogna and Wahr 2006), these assessments carry uncertainties in the order of >10% (Rignot et al. 2011; Zwally and Giovinetto 2011), and even up to 75% (Shepherd et al. 2012), which partly result from large interannual variability in SMB (Wouters et al. 2013). It is then clear that better quantifying Antarctic SMB is essential for the assessment of Antarctic ice sheet mass balance and its contribution to sea level rise, and also for driving ice sheet modeling and depth-age models for ice cores.

The mean Antarctic SMB has been estimated by means of fitting output of regional climate models to in situ observations from snow pits, ice cores, and stake measurements (van de Berg et al. 2006) or interpolating field measurements using remotely sensed data as a background field (Vaughan et al. 1999; Arthern et al. 2006). This results in values of SMB averaged over the grounded Antarctic Ice Sheet ranging from $143\,\mathrm{kg\,m^{-2}\,yr^{-1}}$ (Arthern et al. 2006) to $168\,\mathrm{kg\,m^{-2}\,yr^{-1}}$ (van de Berg et al. 2006), which are usually regarded as the most reliable ones. There may still be uncertainties in these results due to the lack of a robust quality check of the observed SMB data, as performed by Magand et al. (2007) and Favier et al. (2013). In addition, Antarctic SMB has been approximated as precipitation minus surface evaporation/sublimation ($P - E$) using global atmospheric reanalysis products, and also atmospheric global circulation models (e.g., LMDZ4), regional climate models [e.g., Modèle Atmosphérique Régional (MAR), RACMO2, the Polar version of MM5 (PMM5)], and from high-resolution downscaling the output of an atmospheric global climate model (Agosta et al. 2013). However, all these assessments still suffer from considerable uncertainties because of their incomplete parameterizations of polar cloud microphysics and precipitation, and the unsuitability of their physics for cold and snow-covered regions. The magnitude of the uncertainty (equivalent to $\sim$0.25 mm yr^{-1} sea level change; Van Wessem et al. 2014a) is almost as large as the current best assessment of the Antarctic contribution to sea level rise between 1992 and 2011($\sim$0.2 mm yr^{-1}) estimated by Shepherd et al. (2012). Under future climate warming, Antarctic SMB is expected to increase as a result of increased atmospheric moisture content (Krinner et al. 2007; Agosta et al. 2013; Ligtenberg et al. 2013), showing a potentially negative influence on sea level rise in the future (e.g., Krinner et al. 2007; Agosta et al. 2013). However,

most atmospheric climate models and reconstructions combining observations with reanalysis data reveal statistically negligible trends of Antarctic SMB since 1957 (Monaghan et al. 2006a), since 1979 (Lenaerts et al. 2012), and since the early 1980s (Monaghan et al. 2006b; van de Berg et al. 2005). A synthesis of Antarctic SMB from ice core records also shows no significant SMB changes over most of Antarctica since the 1960s, except for an increase in coastal regions with high SMB and the highest part of the East Antarctic ice divide (Frezzotti et al. 2013) and increases in the Antarctic Peninsula (Thomas et al. 2008) and coastal West Antarctica (Thomas et al. 2015).

Multiple studies have attempted to assess the uncertainty of the model outputs using field observations in different regions of Antarctica, such as Adélie Land (Agosta et al. 2012), Fimbul Ice Shelf (Sinisalo et al. 2013), Thwaites Glacier (Medley et al. 2013), and Shirase Glacier drainage basin (Wang et al. 2015). For the whole ice sheet, Bromwich et al. (2011) compared SMB from six reanalysis products with the map based on the interpolation of field observation by Arthern et al. (2006), which contains many unreliable SMB observations. Agosta et al. (2013) evaluated the multiyear averaged SMB of a downscaled SMB product using a quality-controlled and updated compilation of SMB field measurements (Favier et al. 2013), but a temporal variability assessment is lacking. We conclude that it is still necessary to make a comprehensive comparison between observed and simulated SMB from recent reanalyses and regional atmospheric models. This will help to reduce the model uncertainty and to support future model development by identifying biases and shortcomings of the current models.

Our objective is to evaluate to what extent the recent reanalyses and regional atmospheric climate models capture spatial, intra-annual, and interannual variability in Antarctic SMB by comparing them to quality-controlled in situ stake network measurements, ice core records, and weather station observations.

2. Data and methods

a. High-resolution atmospheric climate models

In this study, SMB observations, which are the sum of precipitation, ablation, and wind-driven erosion/deposition, are used to evaluate the temporal and spatial variability in $P - E$ from three global atmospheric reanalyses and three regional climate models: the European Center for Medium-Range Weather Forecasts (ECMWF) interim reanalysis (ERA-Interim), the Modern-Era Retrospective Analysis for Research and Applications (MERRA), the Japan Meteorological Agency

TABLE 1. Summary of the main characteristics of the reanalyses and regional atmospheric climate models.

Model	Organization	Horizontal resolution	Vertical level	Assimilation system	Time coverage
PMM5	PSU–NCAR	—; ~60 km	32	—	1979–2001
JRA-55	JMA	0.5625°; ~60 km	60	4DVar	1955–present
ERA-Interim	ECMWF	0.703125°; ~80 km	60	4DVar	1979–present
MERRA	NASA GMAO	0.5° × 0.667°; ~55 km	72	3DVar	1979–present
RACMO2	KNMI	0.25°; ~27km	40	—	1979–2012

(JMA) 55-Year Reanalysis (JRA-55), the fifth-generation Pennsylvania State University (PSU)–National Center for Atmospheric Research (NCAR) Mesocale Model (MM5) modified for use in polar regions (PMM5), and SMB simulated by two versions of the Regional Atmospheric Climate Model (RACMO2.1 and RACMO2.3). Table 1 summarizes their main characteristics. Note that $P - E$ in the reanalyses and PMM5 is approximated as SMB because wind-driven snow processes are not included. SMB in RACMO2 is the sum of the components including mass increase (precipitation and drifting snow deposition) and mass loss (surface sublimation, drifting snow erosion, and sublimation).

ERA-Interim was generated by the ECMWF to replace the 40-yr ECMWF Re-Analysis (ERA-40), and to prepare the generation of global atmospheric model simulations spanning the entire twentieth century. The reanalysis covers the modern remote sensing data era, from 1979 to the present, and its vertical and horizontal resolutions are 60 levels and T255 (approximately uniform 79 km), respectively. In comparison with ERA-40, significant advances have been made in representing the hydrological cycle and stratospheric circulation, and temporal consistency at different time scales benefited from utilizing the four-dimensional variational (4DVar) analysis system, correcting the bias for satellite radiances, and improving humidity analysis and data handling [for a detailed description, see Dee et al. (2011)].

MERRA from NASA's Global Modeling and Assimilation Office (Bosilovich et al. 2008; Rienecker et al. 2011) was produced using the three-dimensional variational (3DVar) version 5.2.0 of Goddard Earth Observing System Data Assimilation System (GEOS-5) with 72 vertical levels and a spatial resolution of ½° latitude × ⅔° longitude (about 55 km). MERRA output data cover the period from 1979 to present. Great efforts have been made to better represent the large-scale hydrological cycle using an improved land surface hydrological model, corrected precipitation and meteorological forcings based on observations, and the improvements in model physical parameterizations. Bosilovich et al. (2011) reported some improvements of MERRA in the global precipitation, especially over tropical oceans. However,

there are significant biases in the 1990s in high southern latitudes from the addition of Earth Observing System (EOS) data (Cullather and Bosilovich 2011; Bromwich et al. 2011).

JRA-55 was completed in 2013 by JMA for the period from 1958 onward. Many deficiencies found in the first Japanese reanalysis (JRA-25) were removed through the implementation of a new 4DVar data assimilation and prediction system, the introduction of a new radiation scheme and variational bias correction for satellite radiance data, and the use of greenhouse gases history data, three-dimensional daily ozone data, and quality control information drawn from previous reanalyses (Ebita et al. 2011). Increases in computing power also allowed the increase of spatial resolution from T106L40 (nominally 125 km for JRA-25) to TL319L60 (nominally 60 km).

PMM5 is an atmospheric mesoscale model adapted from MM5 for high-latitude use (Bromwich et al. 2001; Cassano et al. 2001). With a resolution of 60 km, PMM5 has been developed over Antarctica forced at the lateral boundaries by ERA-40 for the period January 1979–August 2002 (Monaghan et al. 2006b). Outputs of PMM5 are available online at http://polarmet.osu.edu/.

RACMO2.1 is developed by the Royal Netherlands Meteorological Institute (KNMI), and has been adapted to estimate Antarctic SMB (Van de Berg et al. 2005, 2006; Lenaerts et al. 2012). These adaptations were performed by coupling RACMO2.1 to a snowdrift scheme that describes the interactions of drifting snow with the surface and the lower atmosphere (Lenaerts et al. 2010), an albedo routine with prognostic snow grain size (Kuipers Munneke et al. 2011), and a multilayer snow/ice model that computes melt, percolation, refreezing, and runoff of meltwater (Ettema et al. 2010). The model with a vertical resolution of 40 atmospheric levels and a horizontal resolution ~27 km is forced by ERA-Interim reanalysis data at its ocean and lateral boundaries. Recently, van Wessem et al. (2014a,b) upgraded RACMO2.1 to RACMO2.3 by means of the physics package cycle CY33r1 (ECMWF 2008), which comprises an improved description of turbulent and radiative fluxes, and a change in cloud microphysics, including an ice-supersaturation parameterization.

b. SMB observations

Favier et al. (2013) updated the Antarctic multiyear averaged SMB database constructed by Vaughan et al. (1999) using recent field measurements, which resulted in 5564 observation data. Based on the quality control criteria established by Magand et al. (2007), the updated database was filtered to obtain only the most reliable data (3539 in situ observations) for use in climate studies and climate model evaluation (Favier et al. 2013). We further updated this quality-controlled dataset by adding new field measurements from Fimbul ice shelf (Sinisalo et al. 2013) and the Progress Station–Vostok Station transect (Khodzher et al. 2014), and recalculating SMB along the Chinese traverse route from Zhongshan Station to Dome Argus combining the recent field stake measurements during the period 2008–11 with the previous evaluation by Ding et al. (2011), and the Japanese traverse route between Syowa Station and Dome F according to the improved snow density from Wang et al. (2015). The dataset contains observations averaged for distinct time spans, between several years and several hundred years. Similar to Favier et al. (2013), we used only reliable observations for the past 70 years to correspond with the period (centering on the end of the twentieth century) of the reanalyses and regional climate models. Nevertheless, this does not avoid the biases resulting from multidecadal trends. However, Monaghan et al. (2006a) and Frezzotti et al. (2013) show no significant trends in SMB during the period. The impact is small when compared with spatial variability at a scale of tens of kilometers (details can be seen in section 4). Drifting snow processes are not explicitly included in the reanalyses and PMM5. Because of the inclusion of drifting snow physics in RACMO2, this model run at 5.5 km nicely reproduces negative SMB areas where blue ice areas are observed (Ligtenberg et al. 2014). However, the resolution of RACMO2 we used is 27 km, which is not sufficient to resolve many of the small negative SMB areas, such as the blue ice areas over Taylor glacier. Thus, 190 field observations on these blue ice areas are not included. We account for the observations only covering >5 years of accumulation to remove annual local noise. A subset of 3265 most reliable in situ observations is left to evaluate the model outputs, which are shown in Fig. 1b.

Monaghan et al. (2006a,b) and Frezzotti et al. (2013) have collected long-term accumulation data from ice cores, snow pits, and stake networks to reconstruct the past SMB variability. We update their compilation by addition of stake network observations at Vostok, South Pole, the Japanese traverse route between Syowa Station and Dome F, the ice core data from Law Dome,

Dronning Maud Land (DML), the International Trans-Antarctic Scientific Expedition (ITASE) for West Antarctica during 1999–2002 (Mayewski and Dixon 2013), and Antarctic Peninsula including James Ross Island (Abram et al. 2011), Gomez (Thomas et al. 2008), Dyer Plateau (Thompson et al. 1994), Bryan Coast (Thomas et al. 2015), Ferrigno (Thomas et al. 2015), Jurassic (E. R. Thomas, unpublished data), and Palmer (E. R. Thomas, unpublished data). This update leads to 121 ice cores and stake networks with annual resolution, covering the period 1979–2012 (Fig. 1c). SMB data recorded in individual ice cores can be affected by large postdepositional effects due to the wind-driven processes. The associated spatially small-scale depositional noise can even obscure the accumulation signal for a whole region (Frezzotti et al. 2005; Genthon et al. 2007). Thus, in order to reduce depositional noise, we compute the stacked SMB records of ice cores if they are in the same region, as was also done by Monaghan et al. (2006b). This leaves 33 locations with annually resolved SMB with at least 10 years, of which nine location data are derived from snow stake network measurements and 11 location data are derived from only one ice core. Snow accumulation records from the snow stake network at nine locations are very reliable due to the elimination of local noises through the average across stake farms. Among 11 locations with only one ice core record, seven ice core records are located at Antarctic Peninsula with high snow accumulation ($>700 \, \mathrm{kg \, m^{-2} \, yr^{-1}}$), which allows the evaluation of annual SMB at $\pm 10\%$ accuracy (Frezzotti et al. 2007, 2013). Monaghan et al. (2006b) has reported that single ice cores at Law Dome (LADM) and Siple Dome (SPDM) are representative for the determination of interannual variability in SMB. By omitting the other SMB records from single ice cores that have large local noise, and thus are not representative for regional snow accumulation, 29 in situ observations are left to compare with the interannual variability in simulated SMB, which are indicated in Fig. 1d and Table 2.

c. Methods

Given the high spatial variability in SMB over the Antarctic coastal regions, in situ SMB observations in the same grid cell of JRA-55, ERA-Interim, MERRA PMM5, RACMO2.1, and RACMO2.3 are averaged before comparing the modeled and observed SMB. The mean observed SMB is then compared to the one from the corresponding model grid. We also compare the observation and model output in 200-m elevation bins. Furthermore, the interannual variability in modeled SMB is evaluated using snow accumulation records at 29 sites shown in Fig. 1d. The temporal comparison between
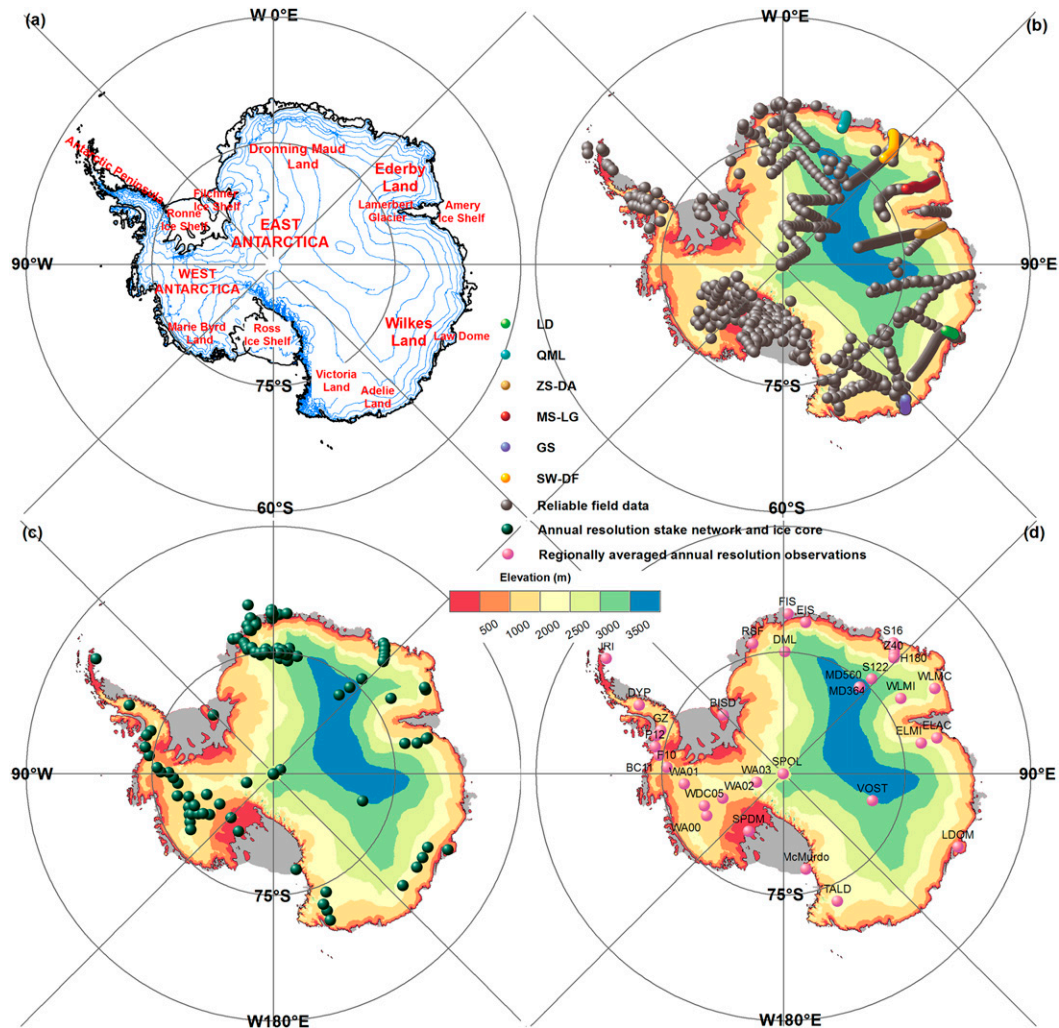
FIG. 1. (a) Map of Antarctica showing the main sites and regions cited in the text. Elevation contours at 500-m intervals from Bamber et al. (2009). (b) Location of updated quality-controlled SMB data in Antarctica, and selected subdatasets for model validation. LD = Law Dome; GS = GLACIOCLIM Surface Mass Balance of Antarctica (GLACIOCLIM-SAMBA) network; SW-DF = Syowa Station–Dome F; ZS-DA = Zhongshan Station-Dome A; MS-LG = Mawson–interior Lambert Glacier; QML = Queen Maud Land. (c) Ice core and stake network sites (dark green dots). (d) Location of annual resolution snow accumulation records after they have been filtered and regionally averaged (pink dots).

in situ observations and SMB simulation is performed only for overlapping time periods, when available. The reanalyses (JRA-55, ERA-Interim, and MERRA), PMM5, and RACMO2.3 are interpolated to the 29 observation locations from the four nearest grids to result in the corresponding temporal series of SMB.

3. Results

a. Comparison of multiyear averaged modeled and observed SMB

The global reanalyses and regional climate models are significantly correlated spatially with in situ observations

($p < 0.01$) over the whole ice sheet, with a correlation coefficient (r) of 0.83 for RACMO2.3, 0.82 for JRA-55, 0.81 for RACMO2.1, 0.80 for ERA-Interim, 0.76 for PMM5, and 0.76 for MERRA (Table 3). Even for the Antarctic ice shelves, the model skills in capturing the spatial variability in SMB are still acceptable, with correlation coefficients > 0.70 ($p < 0.01$). The major known features of Antarctic SMB are well reproduced, including the higher values in the coastal areas and SMB values less than $50\,\mathrm{kg\,m^{-2}\,yr^{-1}}$ in the Antarctic interior above 3200-m elevation. We cannot assess the relative performance of these models due to the scarcity of observational data (231 measurements) at the coastal regions

TABLE 2. Summary of annual resolution ice core and snow stake records shown in Fig. 1 and trend slopes calculated for their corresponding time coverage. Slopes with significant confidence level above 90% are shown; an em dash (—) indicates not significant.

Name	Name abbrev.	Observation source	Latitude	Longitude	Period	Trend	References
Dronning Maud Land	DML	Stack of 30 firm cores	74.96°S	0.67°E	1979–97	0.56 ± 0.22	Oerter et al. 2000; Altnau et al. 2015
Finbul Ice Shelf	FIS	Stack of 9 firm cores	70.33°S	1.61°E	1979–2009	—	Schlosser et al. 2012; Schlosser et al. 2014; Altnau et al. 2015
Ekström Ice Shelf	EIS	Stack of 15 firm cores	71.19°S	8.38°E	1979–2006	11.48 ± 3.54	Altnau et al. 2015
Western Lambert basin coastal region	WLMC	Stack of firm cores LGB00 and MGA	68.65°S	60.68°E	1979–94	—	Goodwin et al. 1994; Higham and Craven 1997
Eastern Lambert basin inland region	ELMI	Stack of firm cores DT001, DT085, and LGB69	72.61°S	77.47°E	1979–96	—	Xiao et al. 2001; Wen et al. 2001; unpublished data
Law Dome	LDOM	Stack of cores DSS97, DSS0405, and DSS0506	66.8°S	112.8°E	1979–2005	−6.49 ± 3.53	van Ommen and Morgan 2010
Vostok	VOST	Stake network	78.45°S	106.87°E	1979–2012	—	Ekaykin et al. 2004, 2012
South Pole	SPOL	Stake network	90.00°S	0°	1983–2012	−3.37 ± 1.05	Lazzara et al. 2012
Siple Dome	SPDM	Siple Dome core	81.65°S	148.99°W	1979–94	—	Kreutz et al. 1997
Talos Dome	TALD	Stack of firm cores GV5, GV7, TD and 31DptA	72.90°S	157.00°E	1979–2009	—	Stenni et al. 2002; Frezzotti et al. 2007
Gomez at Antarctic Peninsula	GZ	Gomez core	73.98°S	70.60°W	1979–2006	15.37 ± 4.86	Thomas et al. 2008
Dyer plateau	DYP	Dyer plateau core	70.67°S	64.87°W	1988–2004	—	Thompson et al. 1994; Thomas et al. 2008
James Ross Island	JRI	James Ross Island core	64.20°S	57.69°W	1979–2008	—	Abram et al. 2011
West Antarctic Ice Sheet Divide	WDC05	Stack of WDC05A and WDC05Q ice core	79.47°S	112.11°W	1979–2005	—	Banta et al. 2008
Bryan Coast	BC11	Bryan coast ice core	74.50°S	81.68°W	1979–2010	—	Thomas et al. 2015
Ferrigno glacier	F10	Ferrigno ice core	75.62°S	86.91°W	1979–2010	4.75 ± 2.25	Thomas et al. 2015
Jurassic	J12	Jurassic ice core	73.67°S	73.06°W	1979–2012	—	Unpublished data
Palmer	P12	Palmer ice core	73.86°S	78.17°W	1979–2012	—	Unpublished data
ITASE for West Antarctica during 1999–2000	WA00	Stack of firm cores 99–1, 00–1, 00–4, 00–5, RIDS-A, RIDS-B, and RIDS-C	79.00°S	119.49°W	1979–2000	—	Kaspari et al. 2004; Mayewski and Dixon 2013
ITASE for West Antarctica in 2001	WA01	Stack of firm cores 01–2, 01–3, 01–4, 01–5, and 01–6	77.67°S	96.00°W	1979–2001	—	Kaspari et al. 2004; Mayewski and Dixon 2013
ITASE for West Antarctica in 2002	WA02	Stack of firm cores CWA-D,02–1 and CWA-A	81.91°S	112.19°W	1979–2002	—	Mayewski and Dixon 2013
McMurdo Station	McMurdo	Precipitation observation	77.85°S	166.65°W	2000–2012	—	ftp://amrc.ssec.wisc.edu/pub/mcmurdo/
JARE S16	S16	Stake network	69.03°S	40.05°E	1984–87; 1992–2001; 2004–2006	—	http://ci.nii.ac.jp/vol_issue/nels/AA10788479_ja.html

TABLE 2. (Continued)

Name	Name abbrev.	Observation source	Latitude	Longitude	Period	Trend	References
JARE H68	H68	Stake network	69.19°S	41.06°E	1984–88; 1992–2002; 2005–2006	—	http://ci.nii.ac.jp/vol_issue/nels/AA10788479_ja.html
JARE H180	H180	Stake network	69.59°S	42.00°E	1984–88; 1992–2002; 2005–2006	—	http://ci.nii.ac.jp/vol_issue/nels/AA10788479_ja.html
JARE S122	S122	Stake network	70.02°S	43.13°E	1984–88; 1992–2002; 2005–06	—	http://ci.nii.ac.jp/vol_issue/nels/AA10788479_ja.html
JARE Z40	Z40	Stake network	70.32°S	43.66°E	1984–88; 1992–2002; 2005–06	—	http://ci.nii.ac.jp/vol_issue/nels/AA10788479_ja.html
JARE MD364	MD364	Stake network	74.01°S	43.00°E	1992–2006	—	http://ci.nii.ac.jp/vol_issue/nels/AA10788479_ja.html
JARE MD560	MD560	Stake network	75.76°S	41.44°E	1992–2006	—	http://ci.nii.ac.jp/vol_issue/nels/AA10788479_ja.html

with the elevations from 200 to 1000 m, as pointed out by Favier et al. (2013) and Agosta et al. (2013). This is a common problem in our updated SMB dataset. Despite the good agreement between the models and in situ observations at the large spatial scale, noticeable deficiencies still exist. As shown in the ratio of the reanalysis and regional climate model data divided by the corresponding grid-averaged observations (Fig. 2), all the reanalyses and three regional climate models indicate clear underestimation in northern Victoria Land and coastal regions of eastern DML where we have high density measurements. Compared with the other models, PMM5 has higher outputs, centering in the Antarctica interior. However, the three reanalyses and two RACMO models underestimate precipitation in inland Antarctica, and especially less than 20% (at some locations even >50%) of observed snow accumulation over the highest parts of East Antarctica is reproduced by ERA-Interim.

We make a comparison of observed SMB and model outputs over the grounded Antarctic Ice Sheet for 200-m elevation bins, using observed elevation. Figure 3a confirms that all atmospheric models agree qualitatively well with the altitudinal distribution of SMB observations. In spite of this, large relative differences (>50%) between observation and simulation occur in elevation bins. In the bins above 2000 m, the averaged differences between observed SMB and PMM5 are positive, revealing a general overestimation of SMB in this model, while differences remain negative for other models, suggesting an underestimate of precipitation over East Antarctica. (Fig. 3b). While precipitation on the East Antarctic Plateau at elevations above 3000 m is underestimated by JRA-55, MERRA, ERA-Interim, and RACMO2.1, this feature is clearly improved in JRA-55. Moreover, Bromwich et al. (2011) present an excessively high precipitation in JRA-25 over the East Antarctic Plateau (>60% overestimate). Obviously, this has been diminished in JRA-55. Among all the models, RACMO2.3 shows the best quantitative agreement with the multiyear averaged measurements, although the model values are still lower than the observed ones. This improvement can be attributed to the updates in the cloud microphysics and large-scale circulation patterns (van Wessem et al. 2014a).

Considering the spatial density of observations, several specific areas where observations cover the same temporal spans and come from the same origin, including Adélie Land (AL), Law Dome (LADM), Zhongshan Station-Dome A (ZS-DA), the west side of Lambert glacier to Mawson Station (MS-LG), Syowa Station-Dome F (SW-DF) and coastal DML (Fig. 1b) are regarded by Favier et al. (2013) as particularly valuable in

TABLE 3. Summary of surface mass balance comparison result.

Modeled SMB	Observations ($n = 3265$)		Observations within the modeled time period ($n = 2430$)		Observations within the modeled time coverage + match time ($n = 2430$)	
	Correlation	Regression slope	Correlation	Regression slope	Correlation	Regression slope
ERA-Interim	0.82	0.77 ± 0.02	0.76	0.74 ± 0.05	0.80	0.75 ± 0.05
MERRA	0.76	0.81 ± 0.03	0.65	0.74 ± 0.07	0.63	0.75 ± 0.07
JRA-55	0.82	0.89 ± 0.02	0.77	0.76 ± 0.05	0.81	0.85 ± 0.05
RACMO2.1	0.81	0.94 ± 0.03	0.76	0.87 ± 0.04	0.83	0.97 ± 0.05
RACMO2.3	0.83	0.88 ± 0.02	0.78	0.79 ± 0.04	0.82	0.86 ± 0.03
PMM5	0.76	0.98 ± 0.04	0.88*	1.14 ± 0.07*	0.88*	1.05 ± 0.06*

* Calculated from 1653 in situ observations.

obtaining information of climate model quality in coastal areas. Figure 4 shows the comparison between the modeled and observed SMB spatial patterns in these special areas. To uniformly compare with the datasets, reanalysis and regional climate model data are bilinearly interpolated on a 20 km × 20 km grid. All models underestimate precipitation over LADM and the coastal DML, despite their good agreement with observed spatial variability. Furthermore, all climate models fail to capture the increasing trend in

SMB at the distance interval ~200–~400 km for the SW-DF transect, and ~70–~120 km from the coast for ZS-GA transect, respectively. PMM5 does not represent the spatial variation pattern from the coast to inland over ZS-DA, MS-LG, and SW-DF. It can be clearly seen from the SMB assessment by RACMO2.3 including snowdrift computation that blowing snow negatively contributes to the SMB in the coastal and katabatic regions, but also that its effect on the SMB spatial pattern is relatively limited.
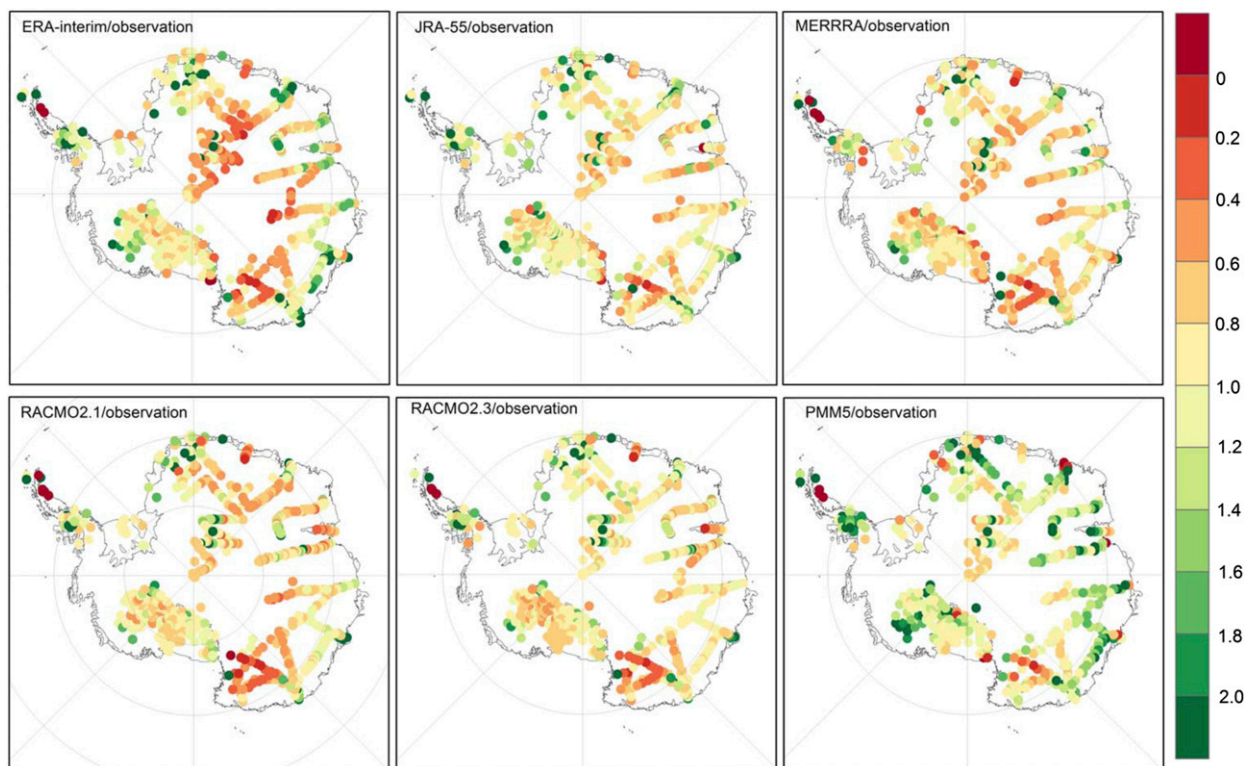

FIG. 2. Simulated and observed SMB. The maps show the ratio of the reanalysis and regional climate model data divided by grid-averaged observation data. It is noted that each spot is at the center of a model grid cell.
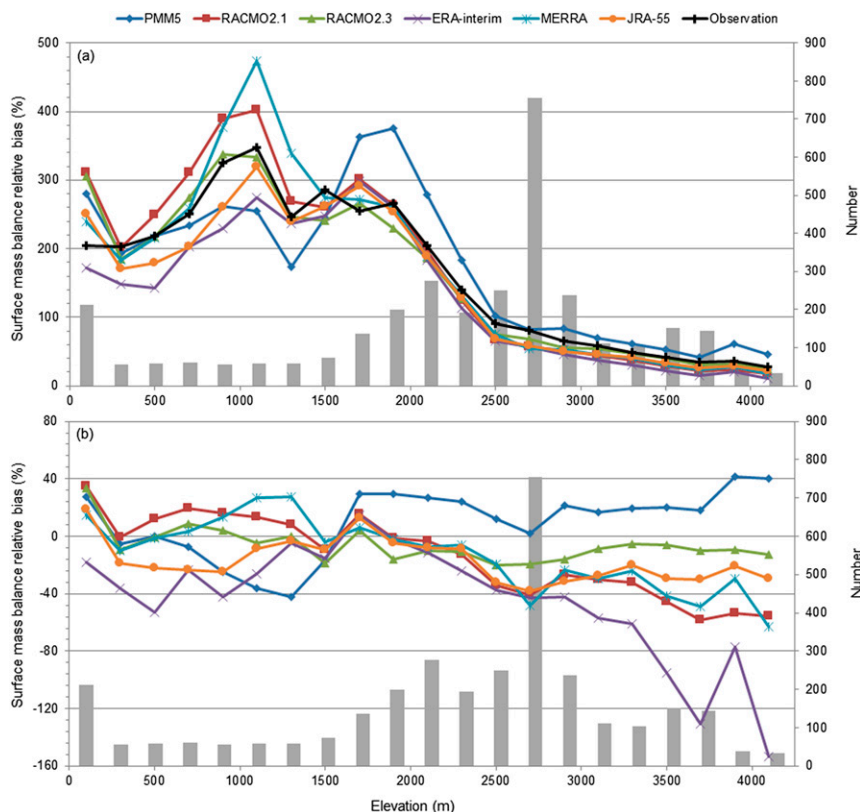
FIG. 3. (a) Comparison of simulated and observed SMB over the grounded ice sheet as a function of elevation. (b) Model bias relative to observed SMB [(model − observation)/(model × 100%)] calculated for each 200-m elevation bin. The bar charts in (a) and (b) denote the number of observations in each elevation bin.

b. Comparison of temporal variability in modeled and observed SMB

1) SEASONAL CYCLE IN MODELED AND OBSERVED SMB

Knowing the seasonal cycle of precipitation is useful for interpreting stable water isotopic composition records from Antarctic ice cores. In situ accumulation observations are sparse, and reanalyses and regional climate models are often used to determine the seasonality of SMB. However, the extent to which they reproduce SMB temporal variability has not been extensively evaluated. Sufficiently long-time series of accumulation observations (at least 5–10 yr) are a prerequisite for the determination of seasonal cycle of snow accumulation over Antarctica (Schlosser 1999; Jouzel et al. 2003). Therefore, we use the gauge measurements of precipitation corrected by stake network observations at Vostok between 1979 and 2012 (available at http://south.aari.nw.ru/) and at McMurdo Station during the period 2000–12 of the Antarctic Meteorological Research

Center (AMRC) and Automatic Weather Station (AWS) program, and stake network measurements at South Pole between 1983 and 2012 (Lazzara et al. 2012). Corrected gauge measurements of precipitation at Vostok are used due to its agreement with accumulation from a stake network at Vostok station (Ekaykin et al. 2004). Figure 5 shows the averaged seasonal distribution of SMB or precipitation from in situ observations and the climate models (ERA-Interim, JRA-55, MERRA, RACMO2.1, and RACMO2.3) for the respective observation periods. Year-to-year variability is large for all the monthly precipitation or SMB at the three sites. Seasonality of accumulation shows a strong similarity at the South Pole and Vostok, with low values in summer. At McMurdo station, precipitation rate peaks in the autumn months [March–May (MAM)], with the lowest values in winter and summer. JRA-55, MERRA, RACMO2.1, and RACMO2.3 agree qualitatively well with the observed SMB seasonal variability at South Pole, while ERA-Interim shows an increase in the summer months. For Vostok and McMurdo, the comparisons are inconclusive because of the large standard deviation in the observations,

FIG. 4. SMB comparison along traverses from the coast to interior Antarctica: (a) AL observaion transect, (b) SW-DF transect, (c) ZS-DA transect, (d) LADM, (e) MS-GL (the traverse along the west side of Lambert glacier from Mawson Station), and (f) DML (the traverse at coastal Dronnig Maud Land) (abbreviations are as in Fig. 1).

although RACMO2.1, RACMO2.3, and ERA-Interim are clearly too wet in winter at McMurdo.

2) INTERANNUAL VARIABILITY IN MODELED AND OBSERVED SMB

Temporal correlation coefficients of observed and simulated annual accumulation are shown in Fig. 6. ERA-Interim has the highest correlation coefficient ($r = 0.5$, $p < 0.05$) with ice core recorded SMB in the west Lambert basin (WLMC), while for the east Lambert basin (ELMI), MERRA present the highest skill for capturing the interannual variation of observed SMB (Fig. 6). The signal of SMB at Vostok and the South Pole is highly reliable because the averaged stake records in the stake networks reduce local noise in SMB. RACMO2.3 fails to represent the interannual variation of observed SMB at Vostok whereas the other datasets correlate well with the observations. Although at the South Pole only ERA-Interim and PMM5 reproduce the negative temporal trend in SMB (Table 2), the correlation coefficients show that JRA-55 and RACMO2.3 present some skill in capturing interannual variability. All the models qualitatively reproduce the chronology of interannual variability at Law Dome with correlation coefficients >0.5 ($p < 0.05$). Except for JRA-55 and RACMO2.1, the correlations for ERA-Interim, MERRA, and RACMO2.3 are significant at Talos Dome (TALD).

In western Dronning Maud Land (DML), a set of 76 firn cores is divided into four subgroups according to geographical region. Stacked records of SMB are calculated for each subgroup (Altnau et al. 2015). Because of the limited temporal coverage (1979–88) of the ice core record at Ritscherflya, we do not include this record in our comparison. All the models, with the exception of RACMO2.3, simulate the interannual variability in SMB over Ekström Ice Shelf (EIS) well. However, all the models fail to do so for Fimbul Ice Shelf (FIS). For this interior location of DML (IDML), only ERA-Interim and RACMO2.1 perform well. Along the Japanese Antarctic Research Expedition (JARE) traverse route from Syowa station to Dome F in eastern DML, long-term snow accumulation measurements by stake farms at all seven locations are reproduced by ERA-Interim, at six locations by RACMO2.3 and JRA-55, at five locations by MERRA, at three locations by PMM5, and at only one location by RACMO2.1.

The 11 remaining locations are located in West Antarctica. All models perform well for simulating observed SMB by ITASE for West Antarctica at 2001 (WA01), ITASE for West Antarctica at 2002 (WA02), and Siple Dome with correlation coefficients above 0.5 ($p < 0.05$), while only ERA-Interim captures the correct sign of interannual change in SMB over ITASE for West Antarctica during 1999–2000 (WA00). On the West Antarctic Ice
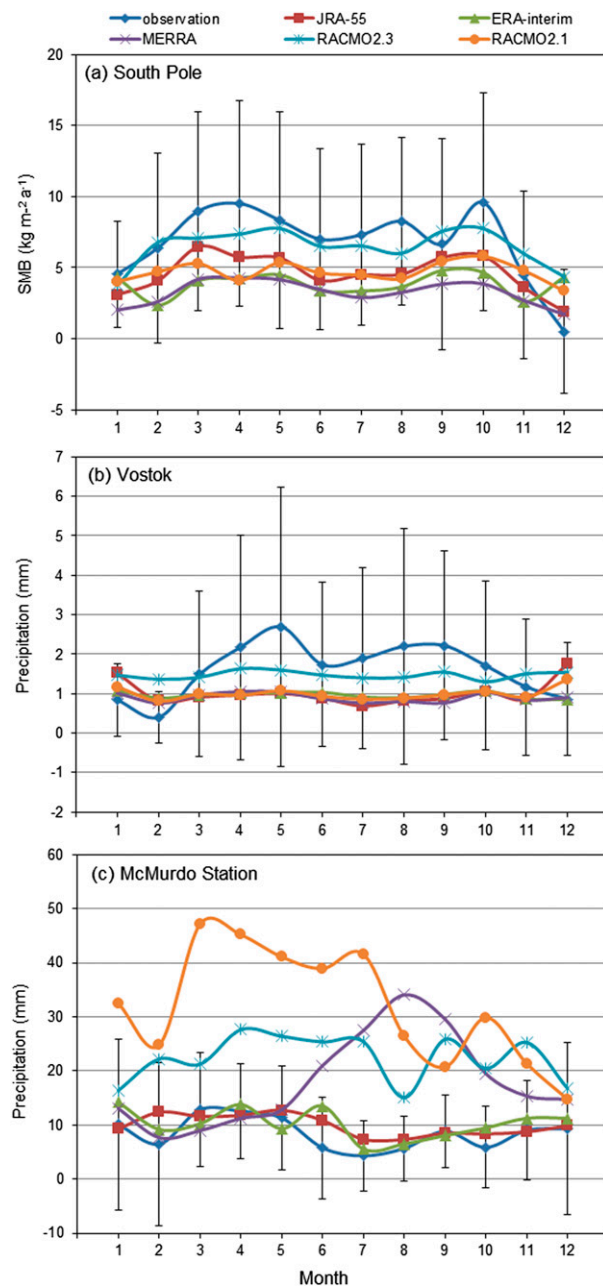
FIG. 5. A comparison of modeled and observed monthly (a) surface mass balance at the South Pole, and precipitation at (b) Vostok and (c) McMurdo stations.

Sheet Divide (WDC05), three reanalysis products and PMM5 perform well, while RACMO2.1 and RACMO2.3 fail to do so. At three of seven locations in the Antarctic Peninsula, all models correlates significantly with the observations. PMM5 and JRA-55 have no significant correlation with Palmer (P12) and Ferrigno (F10) ice core accumulation records. All models reproduce the interannual SMB variability in the Gomez (GZ) and Dyer

Plateau (DYP), except RACMO2.3 and JRA-55, respectively.

In summary, ERA-Interim reproduces the interannual variability in snow accumulation with the highest skill, showing significant correlations with the observations at 28 of 29 sites. Furthermore, its correlations at 15 locations are higher than those of the other five models. JRA-55 captures interannual variability better than ERA-Interim at six out of 29 sites. MERRA correlates significantly with observations at 20 of 29 locations. RACMO2.3 captures variability at some locations (SPOL, WA01, SPDM, and GZ), but fails to do so in 9 of 29 locations. At 15 locations, SMB interannual variability is not represented by RACMO2.1. Robust correlation at more locations of RACMO2.3 than RACMO2.1 may promise some improvement in the RACMO2.3 SMB temporal variability, which is in contrast with the conclusion of insignificant change in performance for interannual variability in relative to RACMO2.1 drawn by a comparison with GRACE satellite retrievals (van Wessem et al. 2014a). Here it is important to note that these versions of the regional climate models do not assimilate data inside their model domain. Future versions will have such an option, which significantly improves temporal variability (van de Berg and Medley 2016).

c. Intercomparison of temporal variability in modeled SMB

1) SEASONAL CYCLE OF SMB SIMULATION

Figure 7a shows the mean annual cycle of precipitation over the Antarctic ice sheet from the reanalyses and regional climate models. We select precipitation to avoid a SMB bias due to sublimation and runoff in summer. Seasonal variability is consistent among all the atmospheric models, with dominant precipitation in autumn (MAM) and smallest precipitation in summer [December–February (DJF)]. We also present the seasonality of SMB components simulated by RACMO2.3 (Fig. 7b). Runoff (not shown) is almost zero on the Antarctic ice sheet because nearly all meltwater that is produced along the margins of the ice sheet refreezes into the snowpack, and melt does not occur in the interior at all. Despite the local importance, deposition/erosion due to the wind divergence/convergence (not shown) ($\sim$4 Gt yr^{-1}; van Wessem et al. 2014a) is minor when averaged over the whole ice sheet, contributing negligibly to the SMB ($\sim$1793 Gt yr^{-1}; van Wessem et al. 2014a). Other SMB components demonstrate a clear annual cycle that exceeds interannual variability. The interannual variability is large for precipitation in each month, but minor for drifting snow and surface sublimation. In spite of the large interannual variability,
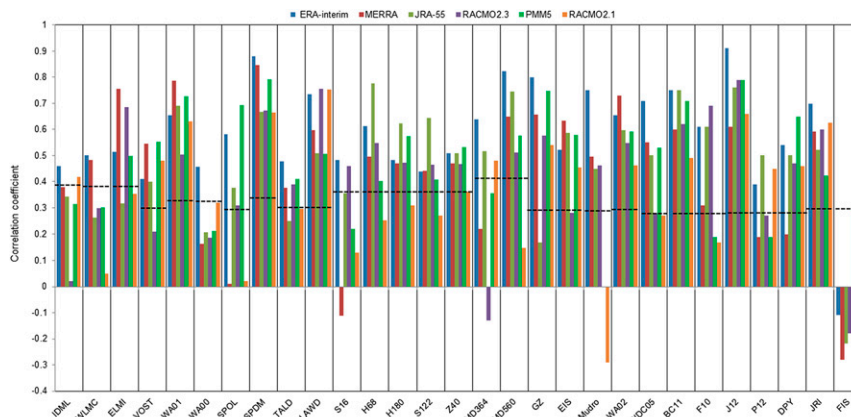
FIG. 6. Correlation coefficient between simulated and observed annual snow accumulation at (dashed lines show the correlation is significantly different from zero at the 90% confidence interval). IDML: inland Droning Maud Land, EIS: Ekström Ice Shelf, WLMC: western Lambert basin coastal region, ELMI: eastern Lambert basin inland region, LDOM: Law Dome, VOST: Vostok, SPOL: South Pole, SPDM: Siple Dome, TALD: Talos Dome, GZ: Gomez ice core at Antarctic Peninsula, JRI: James Ross Island, WDC05: West Antarctic Ice Sheet Divide, BC11: Bryan Coast, F10: Ferrigno glacier, J12: Jurassic, P12: Palmer, WA00: ITASE for West Antarctica during 1999–2000, WA01: ITASE for West Antarctica at 2001, WA02: ITASE for West Antarctica at 2002, McMurdo: McMurdo Station; also, S16, H68, H180, S122, Z40, MD364, and MD560 are stake network sites along Japanese Antarctic Research Expedition traverse route.

precipitation shows a significant minimum in summer months and maximum in autumn months. Surface sublimation increases from the end of spring and peaks in summer; its values are near zero in the other months. Drifting snow sublimation seasonality agrees well with that based on RACMO2.1 (Lenaerts et al. 2012), with higher values in autumn and spring. Influenced by the higher wind speeds in winter and the occurrence of melt in summer, drifting snow sublimation increases from the short summer (December and January) to midwinter.

Figure 8 illustrates the spatial distribution of precipitation seasonality over the Antarctic Ice Sheet and

surrounding ocean. Seasonality of precipitation in many areas of the ice sheet is comparable among the models. Coastal regions are characterized by low precipitation in summer. The highest precipitation is found during autumn in the eastern DML coastal regions, Lambert glacier, and large regions of the Antarctic interior. Wilkes Land receives most precipitation in winter [June–August (JJA)]. Despite being consistent, ERA-Interim and PMM5 show a distinctly different seasonality from the observations over the large parts of the East Antarctic plateau, with high precipitation in summer, whereas observations show a snowfall minimum in this season
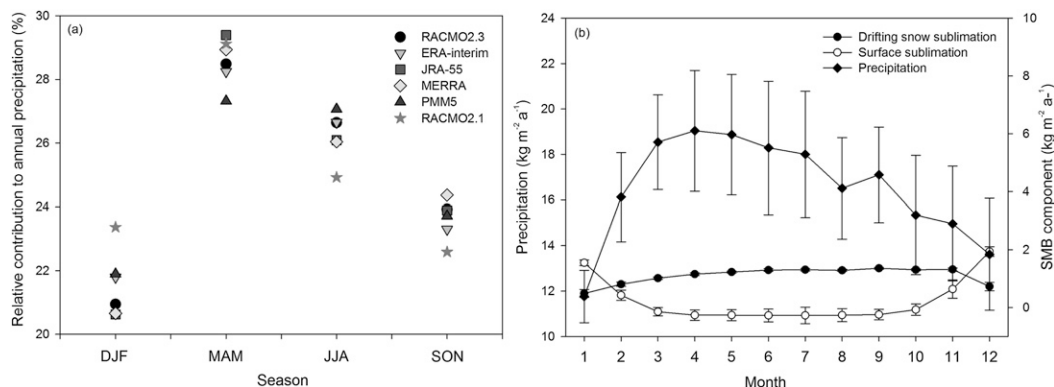

FIG. 7. (a) Seasonal contribution to annual averaged precipitation of PMM5 for the period 1979–2001, and JRA-55, ERA-Interim, MERAA, and RACMO2.3 for the period 1979–2012. (b) Monthly averaged surface mass balance components between 1979 and 2013 by RACMO2.3.
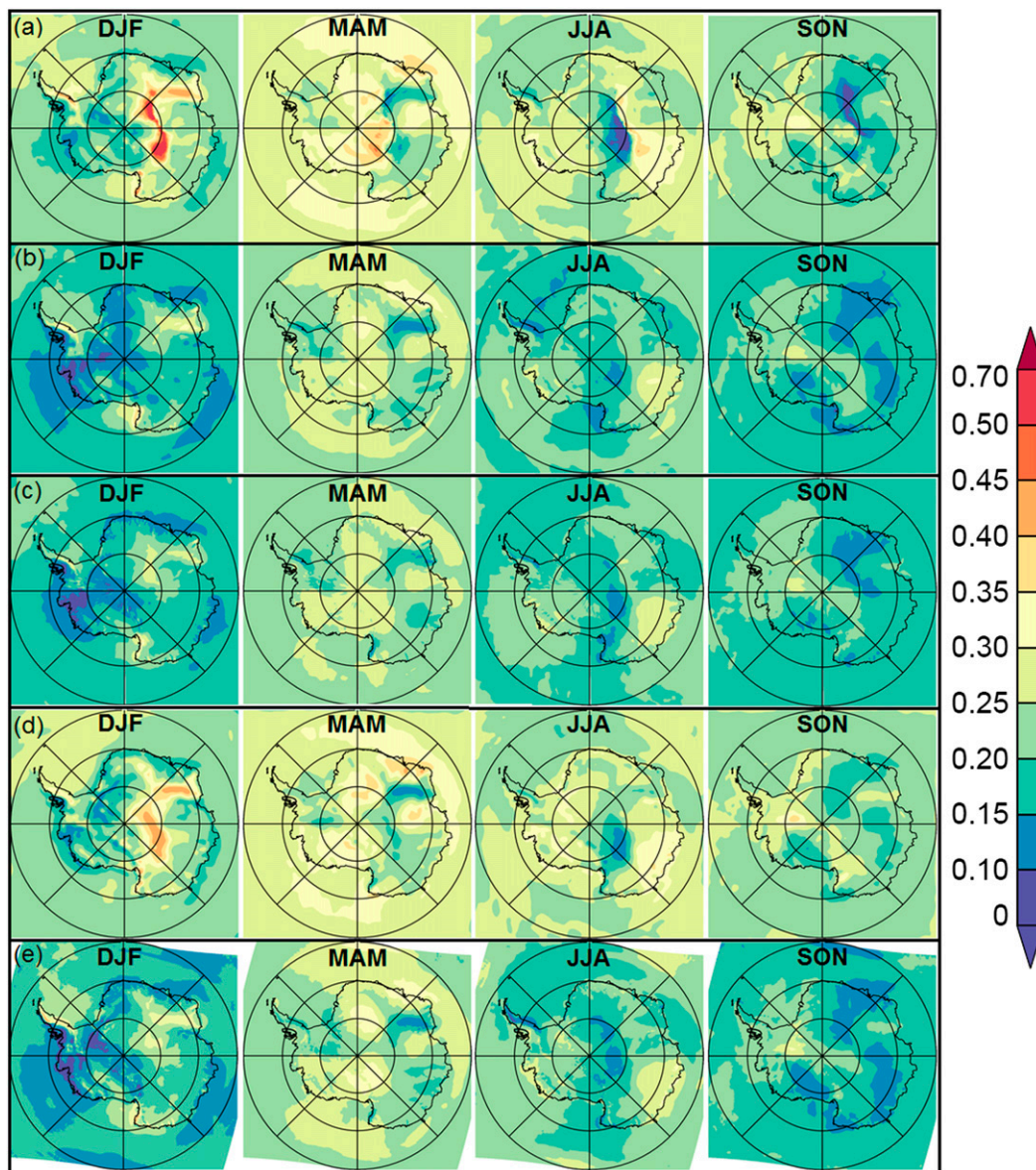
FIG. 8. Spatial patterns of contribution of seasonal precipitation to annual mean from (a) ERA-Interim, (b) JRA-55, (c) MERRA, (d) PMM5, and (e) RACMO2.3. The average spans from 1979 to 2012 for ERA-Interim, JRA-55, MERRA, and RACMO2.3; the averaged time period for PMM5 is 1979–2001.

([Laepple et al. 2011](#)). In addition, over Enderby Land, the precipitation seasonality in ERA-Interim and PMM5 strongly peaks in austral summer.

2) INTERANNUAL VARIABILITY OF SMB SIMULATION

The time series of annually and spatially integrated SMB are shown as deviations from the temporal mean between 1981 and 2001 ([Fig. 9a](#)). When calculating Antarctic SMB, we use the ice sheet mask from Antarctic Digital Database (ADD) version 6.0 (http://www.add.scar.org/).

Large interannual variability is common for all the reanalyses and regional climate models. JRA-55 exhibits a ~6% increase in annual precipitation averaged between 1999 and 2012, relative to the period from 1979 to 1998. Although this is smaller than the upward shift in the late 1990s (~10% precipitation increase) reported by [Bromwich et al. (2011)](#), it is still spurious. There is also a significant discontinuity for JRA-55 $P - E$ time series before and after 1979 ([Fig. 9b](#)). The $P - E$ values over the whole continent increase by ~19% for 1979–2012 in relation to 1959–79. The changes are larger from low
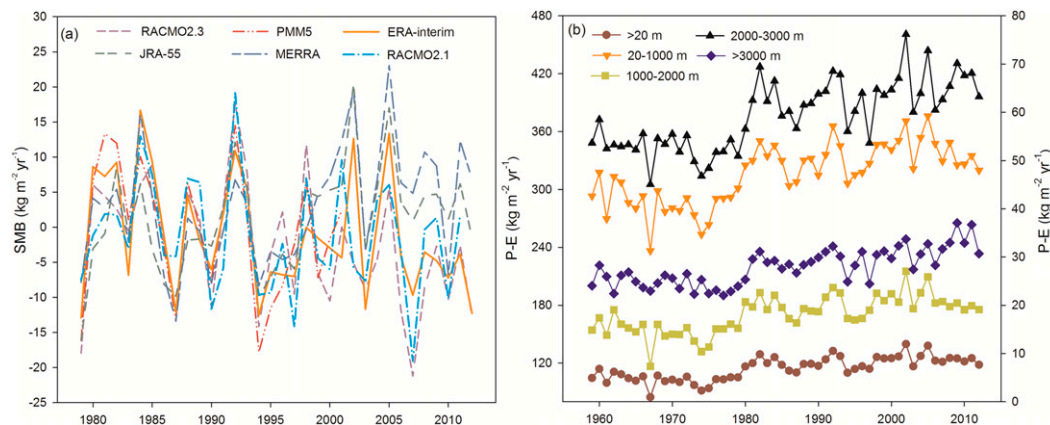
FIG. 9. (a) Time series of annual SMB averaged over the Antarctic Ice Sheet. (b) Annual mean JRA-55 Antarctic forecast precipitation minus evaporation $(P - E)$ for various regions with different elevations. $P - E$ values at the elevation bins of $>20\,\mathrm{m}$, 20–1000 m, and 1000–2000 m are shown on the left axis, and $P - E$ values at other elevation bins are shown on the right axis.

elevation bins to the continental interior with the highest elevations, where $P - E$ increases reach more than 22%.

Linear trends are evaluated (not shown), and their significance is computed by the p value of a two-tailed Student's t test. For average Antarctic SMB, there is no significant trend in ERA-Interim during the period 1979–2012 and PMM5 during the period 1979–2001, which agrees with the observation-based results of Monaghan et al. (2006a) and Frezzotti et al. (2013). For 1979–2012, large positive trends occur in MERRA and JRA-55, significant at the 95% confidence level, while RACMO2.3 shows a significant negative trend ($p < 0.05$). The sign of the changes of RACMO2.3 is consistent with RACMO2.1, but the SMB trend in RACMO2.1 is insignificant.

The spatial distribution of trends in SMB simulated by ERA-Interim, JRA-55, MERRA, PMM5, RACMO2.1, and RACMO2.3 shows important regional differences (Fig. 10). It is obvious that the magnitude and spatial extent of trends differ substantially among the models. Probably because of the low temporal coverage (1979–2001), the spatial extent of PMM5 demonstrates less significant trends than the other reanalyses and regional climate models. Three reanalyses show larger regions with significant trends over DML than the three regional climate models, and a clear significant trend over Wilkes Land occurs in RACMO2.3. In particular, significant positive trends in western coastal DML (including Fimbul Ice Shelf) are found in JRA-55, MERRA, RACMO2.1, and PMM5. However, the composite of ice core records at Fimbul Ice Shelf shows a negative accumulation trend between 1979 and 2009 (Fernandoy et al. 2010; Altnau et al. 2015). Only JRA-55 shows significant trends in the main East Antarctic ice divides,

in accordance with the SMB increase since the 1960s observed by Frezzotti et al. (2013).

Some similar trend patterns can be found in several or even all the models. In the 45°–145°E sector of coastal East Antarctica, similar patterns occur in ERA-Interim, PMM5, RACMO2.1, and RACMO2.3, with a positive trend in Enderby Land, and negative trend in central Wilkes Land. Furthermore, the models capture the negative trend during the period 1979–2005 over Law Dome (van Ommen and Morgan 2010). JRA-55 and MERRA demonstrate the same trend at Enderby Land as in ERA-Interim, RACMO2.1, and RACMO2.3, but a positive trend over central Wilkes Land. This is consistent with the increase since the 1960s reported by Frezzotti et al. (2013). All datasets have statistically significant negative trends over Adélie Land, which may originate from the enhanced off-continent winds (Bromwich et al. 2011). In general, there are no statistically significant trends over West Antarctica. However, Thomas et al. (2015) reported a significant increase in the coastal areas of West Antarctica. All models capture the positive trends in the Gomez ice core region (Thomas et al. 2008) but fail to reproduce the significant negative trends in accumulation found at five ice core sites over the West Antarctic ice sheet divide during the period 1975–2010 (Burgener et al. 2013).

4. Discussion

The observations are averaged over different time periods. They are not rescaled to the temporally unbiased mean SMB of the atmospheric models when performing the spatial comparison between observation and simulation. Therefore, spatial differences in accumulation
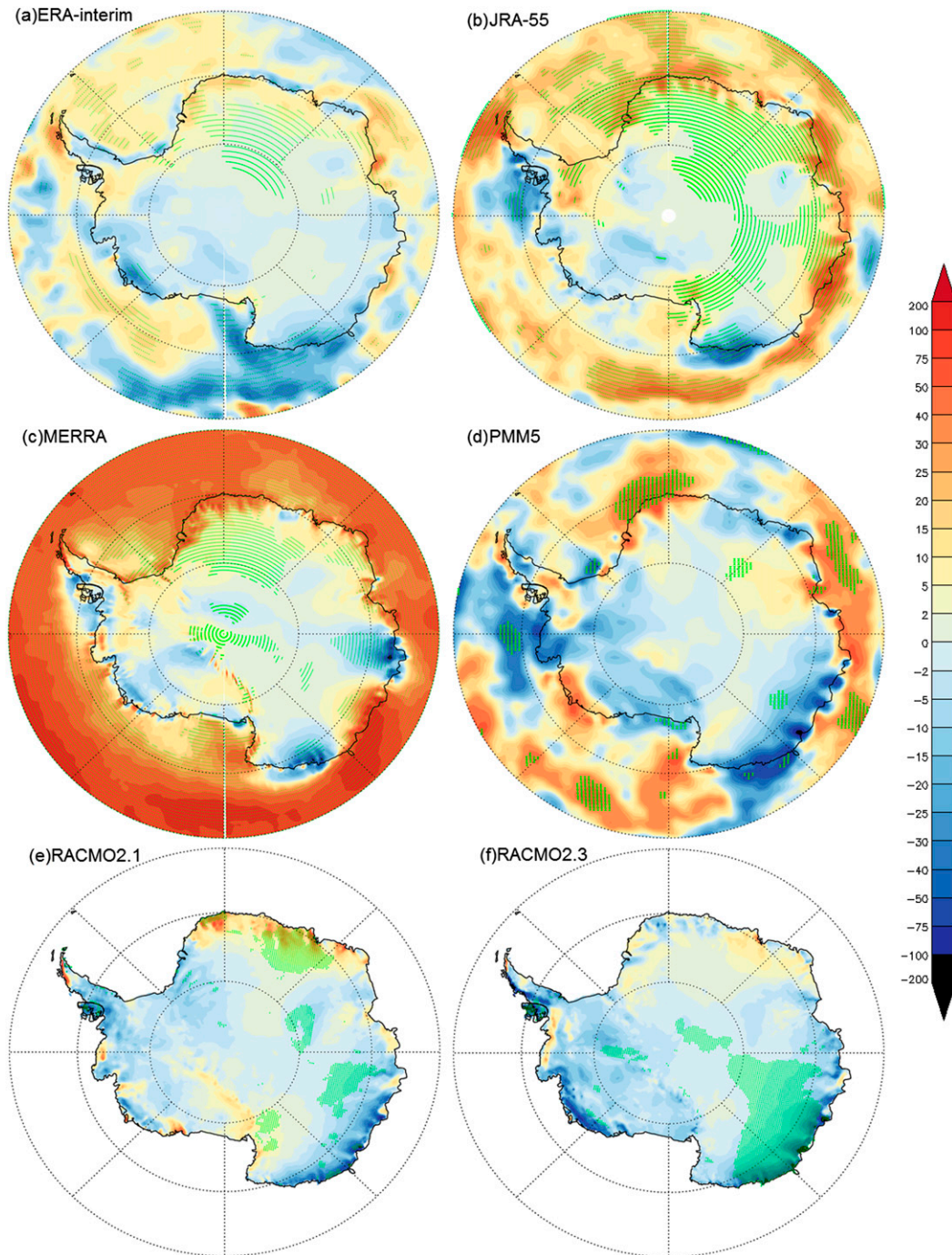
FIG. 10. Spatial distribution of linear trends for each model grid (mm yr^{-1} decade^{-1}). Dotted regions show trends that are statistically significant at the 95% confidence level. Over the open ocean for (a) ERA-Interim, (b) JRA-55, (c) MERRA, and (d) PMM5 the $P - E$ trends are indicated.

values may partly result from temporal changes in snow accumulation. We filter observations with time periods covered by MERRA, ERA-Interim, JRA-55, RACMO2.1, and RACMO2.3 (1979–2012) and by PMM5 (1979–2001) to quantify the influence of temporal mismatch on spatial

variation comparison between SMB observations and simulation. This leads to a decrease in the number of observations due to their wide variety of accumulation time periods. As Table 3 shows, the observations correlate to the SMB simulation by MERRA with a correlation

coefficient of 0.65. When compared with MERRA-simulated SMB for the exact time period covered by the observations, the correlation declines slightly to 0.63. The regression slope increases by only 0.01. For PMM5, the correlation does not vary, and there is no significant change in the regression slope either. In terms of other reanalysis products and regional climate models, the correlation between observation and simulation resulting from ignoring temporal variability decreases by 0.04–0.07. Furthermore, the decrease in regression slopes ranges from 0.01 to 0.11. This suggests differences in accumulation values originating from a changing accumulation rate over several decades are small compared to spatial variability at a scale of tens of kilometers. Therefore, the impact of temporal inhomogeneity on our spatial variability estimate of SMB simulation using observations can be neglected.

Although the reanalysis products and three regional climate models are qualitatively consistent with SMB measurements on the large spatial scale, there are still noticeable differences such as overestimation in AL, parts of ZS-DA, SW-DF, and MS-LG for three regional climate models, and underestimation in northern Victoria Land, Law Dome, and coastal DML for all models. The overestimations in some coastal regions of the ice sheet may be explained by the artificial diffusion-enhanced moisture transport along model levels, which results in an uphill moisture transport (van de Berg et al. 2005). This is a common problem of atmospheric models in areas with steep topography (Connolley and King 1996; Van Lipzig and van den Broeke 2002; Lenderink et al. 2003; van de Berg et al. 2006). Model resolution and difference between model and surface elevation may also contribute to the observed and modeled SMB differences (Agosta et al. 2012). In addition, reanalysis models are not optimized for snow-covered regions. Their surface scheme does not include complex parameterizations of snowpack processes and their atmospheric physics may perform poorly under cold conditions (very stable boundary layers, cloud microphysics). As a result, unrealistic precipitation during the long winter in inland Antarctica probably occurs in ERA-Interim (Fig. 8).

Over the East Antarctic plateau, ERA-Interim, MERRA, and RACMO2.1 indicate an overall underestimate of precipitation, while JRA-55 improves this. This may be related to the first assimilation of the newly reprocessed atmospheric motion vectors (AMVs) and clear-sky radiances (CSRs) from the Geostationary Meteorological Satellite (GMS) and Multifunctional Transport Satellite (MTSAT) with high quality, which is performed by the JMA Meteorological Satellite Center (MSC). The >~50% precipitation underestimate in ERA-Interim can be improved using the atmospheric
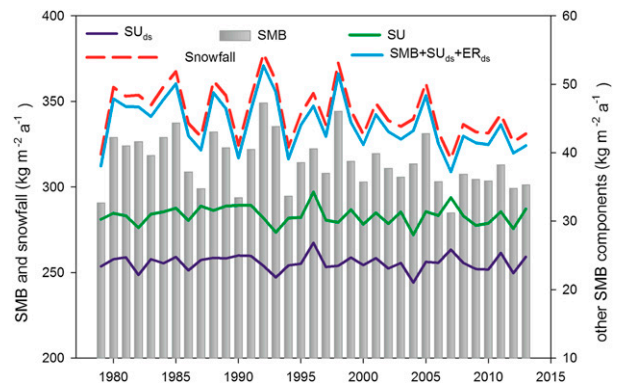

FIG. 11. Time series of SMB components over the Antarctic Ice Sheet below 2000-m elevation between 1979 and 2013 from RACMO2.3. Values for SMB, snowfall, and SMB without wind-driven snow processes are indicated by the left axis, and values for the other SMB components are indicated by the right axis. SU: surface sublimation, SU_{ds}: sublimation of drifting snow, ER_{ds}: erosion by drifting snow.

moisture flux budget method (Bromwich and Wang 2008; Bromwich et al. 2011). However, the large underestimation probably, at least to some extent, results from the unrealistic amounts of inland precipitation during the long Antarctic winter, which leads to a substantial seasonality in precipitation.

Blowing snow sublimation is highly important for SMB in the regions where katabatic winds are strong, and they can even locally remove all annual snowfall, resulting in the formation of blue ice areas (Richardson et al. 1997; Siegert et al. 2003; Frezzotti et al. 2004; Frezzotti et al. 2007; Genthon et al. 2007; Lenaerts et al. 2010; Scarchilli et al. 2010; Arcone et al. 2012; Scambos et al. 2012). Remote sensing and ground traverses have shown that negative SMB regions due to wind scouring covers ~2.7–6.6% of the Antarctic surface area (Das et al. 2013). Based on RACMO2.1 and RACMO2.3 (Lenaerts et al. 2012; van Wessem et al. 2014a), drifting sublimation averaged over the ice sheet in magnitude accounts for ~10% of annual precipitated snow. This value is comparable to that derived from the MAR (Gallée et al. 2013b). Nevertheless, according to the blowing snow flux comparison between simulation and observation (Gallée et al. 2013a), it could actually be twice as large. It is also clearly seen in Fig. 4 that the drifting snow sublimation and deposition/erosion from wind divergence/convergence contribute negatively to regional SMB, but their influence on the spatial variability pattern is limited. We further examine the influence of blowing snow processes on interannual variability in SMB at the Antarctic Ice Sheet at elevations below 2000 m where wind-driven snow processes are large, based on RACMO2.3 (Fig. 11). There is no significant interannual variability in drifting snow

sublimation and wind-driven erosion/deposition. SMB interannual variability corresponds well with precipitation temporal variability, suggesting the minor influence of blowing snow processes on interannual variability in SMB. We conclude that wind-driven ablation at local and global scales is not negligible and could represent a significant negative contribution to SMB, and thus explain the quantitative difference between SMB observations and simulations, particularly in windy areas. However, the contribution of blowing snow processes to the spatial and interannual variability in SMB at regional scales is very limited.

A good understanding of seasonality of SMB is vital when interpreting stable water isotopic composition in ice cores, used as a proxy for paleo-temperature, especially for the areas where annual variability in precipitation tends to be dependent mainly on one season (Jouzel et al. 2003). All the reanalyses and regional climate models show a precipitation maximum in autumn integrated over the whole Antarctic Ice Sheet, which largely depends on precipitation at coastal regions where cyclone activity is very high in this season. However, on large parts of the East Antarctic Plateau, seasonal accumulation in ERA-Interim has a strong peak in austral summer ($>50\%$ of annual snowfall occurs in this season), which is not in accordance with the observed winter maxima in accumulation in this region (Laepple et al. 2011). Also, long (>10 yr) measurement time series at Vostok and the South Pole have revealed a winter maximum in snow accumulation (Fig. 5). The winter maximum is attributed to clear-sky precipitation, the summer ablation, as well as the increase in moisture transport resulting from the winter weather systems (Bromwich 1988; Ekaykin 2003). However, the performance of the moisture-related atmospheric physics in ERA-Interim may be poor under cold conditions, and result in small snowfall in winter.

Corrections by observations are usually carried out to reduce the uncertainty in the reanalysis forecast models. This process, especially changes in the observing system may produce artificial error or play a role in the water budget, which in turn affects the representation of the hydrological cycle (Kobayashi et al. 2015). The introduction of Advanced Microwave Sounding Unit (AMSU) data in November 1998 is known to afflict MERRA (Cullather and Bosilovich 2011; Bromwich et al. 2011) and the NCEP Climate Forecast System Reanalysis (Saha et al. 2010). The significant increase in JRA-55 precipitation in the late 1990s is probably related to the assimilation of AMSU data. Fifteen ice core accumulation records extending at least back to 1958 allow examination of the performance of JRA-55 for the time span 1959–78. No significant correlation was found at any location during this time period. However, snow accumulation at 12 of the 15 locations correlates significantly with JRA-55 $P - E$ for the period 1979–2012 (Fig. 6). In addition, we compare the correlation between observation and JRA-55 simulation at South Pole and seven sites at the Antarctic Peninsula during the period from 1999 to 2012 relative to 1979–1998. Correlation coefficients at these locations increase by 0.1–0.3 (not shown). This suggests that representation of Antarctic precipitation is greatly dependent on satellite observing systems. Kobayashi et al. (2015) has also pointed out that representation of global precipitation except Antarctica in JRA is more sensitive to satellite observing systems than other reanalyses such as MERRA, JRA-25, ERA-40, and ERA-Interim. Therefore, the positive trend in JRA-55 during 1979–2012 may be also due to the considerable increase in satellite observations after the late 1990s, which result in higher modeled precipitation amounts.

For the period 1979–2012, ERA-Interim reanalysis reveals an insignificant trend in SMB over the Antarctic Ice Sheet, in agreement with the reconstructed SMB by calibrating ERA-40 using ice core records (Monaghan et al. 2006b) and the synthesis of Antarctic snow accumulation records from ice cores (Frezzotti et al. 2013). In particular, among the reanalysis products and regional climate models, ERA-Interim agrees best with interannual variability in the available observations between 1979 and 2012 from the majority of the continent. Therefore, we conclude that the interannual variability and trends in the ERA-Interim precipitation fields are the most reliable of all models studied.

5. Conclusions

This study further updates the recent compilation of the quality controlled multiyear averaged SMB observations by Favier et al. (2013), and annual resolution SMB observations by Monaghan et al. (2006a,b) and Frezzotti et al. (2013). Based on this updated dataset, we assess the skill of JRA-55, ERA-Interim, MERRA, RACMO2.1, RACM2.3, and PMM5 in reproducing the spatial and annual variability in SMB. In addition, the seasonality of the simulated SMB is compared with the observations from three locations and the seasonal and the interannual variability of these simulations are also considered.

In spite of the different time periods spanned by the SMB measurements and the model simulations, the impact of the use of different time periods on our spatial comparison between observations and simulations at a scale of tens of kilometers can be neglected. All atmospheric climate models represent the spatial patterns of

SMB on a continental scale well, with correlation coefficients >0.80 ($p < 0.05$), but we do not rank their relative skills due to the sparse field measurements over the coastal regions with the elevations from 200 to 1000 m. Over the East Antarctic Plateau, precipitation is underestimated by JRA-55, MERRA, ERA-Interim, and RACMO2.1. The underestimate is clearly reduced in JRA-55, compared with MERRA, ERA-Interim, and RACMO2.1, probably associated with the first assimilation of the newly reprocessed AMVs and CSRs from GMS, although its accuracy is still lower than RACMO2.3 for this region.

The three reanalyses (JRA-55, ERA-Interim, and MERRA) and three regional climate models (PMM5, RACMO2.1, and RACMO2.3) agree well with the observed seasonality of precipitation over the Antarctic Ice Sheet, with maximum precipitation in autumn, and minimum in summer; however, in many locations, no conclusion can be drawn about the seasonality of precipitation or SMB from short-term observations due to the uncertainty resulting from year-to-year variability. This makes it difficult to assess atmospheric model simulations. We find that precipitation in ERA-Interim strongly peaks in austral summer over the large areas of the East Antarctic main ice divide region, in contrast to the observed winter maximum in precipitation in this region (Laepple et al. 2011). This may result from the unrealistic winter precipitation amount estimate over the Antarctic interior, which is also a possible reason for dry bias in inland Antarctica in ERA-Interim.

Although JRA-55 is produced using a more advanced assimilation scheme (4DVar), newer variational bias correction (VarBC) for satellite radiances and a higher spectral truncation (TL139, ~60km) than ERA-40, JRA-55 still presents a dramatic jump in Antarctic snow accumulation around 1979, well known to us in ERA-40. In addition, a large increase in annual precipitation occurs in the late 1990s relative to 1979–98. This may be due to the assimilation of quantities of satellite sounding data after 1979, and further increased satellite observations in the late 1990s. Therefore, the large positive and statistically significant SMB trends for the period 1979–2012 in JRA-55 are spurious. The positive trend in MERRA during the same period as JRA-55 is confirmed to be not trustworthy by Bromwich et al. (2011). The skill of the three regional climate models for capturing SMB interannual variability is limited, probably due to the lack of observational data assimilated inside their model domain. Among all the models and reanalysis products, ERA-Interim agrees best with the 29 annual resolution observation records, each of which is representative of a region surrounding it. Therefore, we conclude that ERA-Interim provides the best skill for describing precipitation interannual variability and trend between 1979 and 2012.

REFERENCES

Abram, N. J., R. Mulvaney, and C. Arrowsmith, 2011: Environmental signals in a highly resolved ice core from James Ross Island, Antarctica. *J. Geophys. Res.*, **116**, D20116, doi:10.1029/2011JD016147.

Agosta, C., V. Favier, C. Genthon, H. Gallée, G. Krinner, J. T. M. Lenaerts, and M. R. van den Broeke, 2012: A 40-year accumulation dataset for Adelie Land, Antarctica and its application for model validation. *Climate Dyn.*, **38**, 75–86, doi:10.1007/s00382-011-1103-4.

——, ——, G. Krinner, H. Gallée, X. Fettweis, and C. Genthon, 2013: High-resolution modelling of the Antarctic surface mass balance, application for the twentieth, twenty first and twenty second centuries. *Climate Dyn.*, **41**, 3247–3260, doi:10.1007/s00382-013-1903-9.

Allison, I., R. Alley, H. Fricker, R. Thomas, and R. Warner, 2009: Ice sheet mass balance and sea level. *Antarct. Sci.*, **21**, 413–426, doi:10.1017/S0954102009990137.

Altnau, S., E. Schlosser, E. Isaksson, and D. Divine, 2015: Climatic signals from 76 shallow firn cores in Dronning Maud Land, East Antarctica. *Cryosphere*, **9**, 925–944, doi:10.5194/tc-9-925-2015.

Arcone, S. A., R. Jacobel, and G. Hamilton, 2012: Unconformable stratigraphy in East Antarctica: Part 1. Large firn cosets, recrystallized growth, and model evidence for intensified accumulation. *J. Glaciol.*, **58**, 240–252, doi:10.3189/2012JoJ11J044.

Arthern, R. J., D. P. Winebrenner, and D. G. Vaughan, 2006: Antarctic snow accumulation mapped using polarization of 4.3-cm wavelength microwave emission. *J. Geophys. Res.*, **111**, D06107, doi:10.1029/2004JD005667.

Bamber, J. L., J. L. Gomez-Dans, and J. A. Griggs, 2009: Antarctic 1 km Digital Elevation Model (DEM) from Combined ERS-1 Radar and ICESat Laser Satellite Altimetry. National Snow and Ice Data Center, accessed 12 July 2014, doi:10.5067/H0FQ1KL9NEKM.

Banta, J. R., J. R. McConnell, M. M. Frey, R. C. Bales, and K. Taylor, 2008: Spatial and temporal variability in snow accumulation at the West Antarctic Ice Sheet Divide over recent centuries. *J. Geophys. Res.*, **113**, D23102, doi:10.1029/2008JD010235.

Bentley, C., 1993: Antarctic mass balance and sea level change. *Eos, Trans. Amer. Geophys. Union*, **74**, 585–586, doi:10.1029/93EO00653.

Bosilovich, M. G., J. Chen, F. R. Robertson, and R. F. Adler, 2008: Evaluation of precipitation in reanalyses. *J. Appl. Meteor. Climatol.*, **47**, 2279–2299, doi:10.1175/2008JAMC1921.1.

——, F. R. Robertson, and J. Chen, 2011: Global energy and water budgets in MERRA. *J. Climate*, **24**, 5721–5739, doi:10.1175/2011JCLI4175.1.

Bromwich, D. H., 1988: Snowfall in high southern latitudes. *Rev. Geophys.*, **26**, 149–168, doi:10.1029/RG026i001p00149.

——, and S.-H. Wang, 2008: A review of the temporal and spatial variability of Arctic and Antarctic atmospheric circulations based upon ERA-40. *Dyn. Atmos. Oceans*, **44**, 213–243, doi:10.1016/j.dynatmoce.2007.09.001.

——, J. J. Cassano, T. Klein, G. Heinemann, K. M. Hines, K. Steffen, and J. E. Box, 2001: Mesoscale modeling of katabatic winds over Greenland with the Polar MM5. *Mon. Wea. Rev.*, **129**, 2290–2309, doi:10.1175/1520-0493(2001)129<2290:MMOKWO>2.0.CO;2.

——, J. P. Nicolas, and A. J. Monaghan, 2011: An assessment of precipitation changes over Antarctica and the Southern Ocean since 1989 in contemporary global reanalyses. *J. Climate*, **24**, 4189–4209, doi:10.1175/2011JCLI4074.1.

Burgener, L., and Coauthors, 2013: An observed negative trend in West Antarctic accumulation rates from 1975 to 2010: Evidence from new observed and simulated records. *J. Geophys. Res.*, **118**, 4205–4216, doi:10.1002/jgrd.50362.

Cassano, J. J., J. E. Box, D. H. Bromwich, L. Li, and K. Steffen, 2001: Verification of Polar MM5 simulations of Greenland's atmospheric circulation. *J. Geophys. Res.*, **106**, 33 867–33 890, doi:10.1029/2001JD900044.

Chen, J. L., C. R. Wilson, D. Blankenship, and B. D. Tapley, 2009: Accelerated Antarctic ice loss from satellite gravity measurements. *Nat. Geosci.*, **2**, 859–862, doi:10.1038/ngeo694.

Church, J. A., J. Gregory, P. Huybrechts, M. Kuhn, K. Lambeck, M. Nhuan, D. Qin, and P. Woodworth, 2001: Changes in sea level. *Climate Change 2001: The Scientific Basis*, J. Houghton et al., Eds., Cambridge University Press, 639–693.

Connolley, W. M., and J. C. King, 1996: A modeling and observational study of East Antarctic surface mass balance. *J. Geophys. Res.*, **101**, 1335–1344, doi:10.1029/95JD03034.

Cullather, R. I., and M. G. Bosilovich, 2011: The moisture budget of the polar atmosphere in MERRA. *J. Climate*, **24**, 2861–2879, doi:10.1175/2010JCLI4090.1.

Das, I., and Coauthors, 2013: Influence of persistent wind scour on the surface mass balance of Antarctica. *Nat. Geosci.*, **6**, 367–371, doi:10.1038/ngeo1766.

Dee, D. P., and Coauthors, 2011: The ERA-Interim reanalysis: Configuration and performance of the data assimilation system. *Quart. J. Roy. Meteor. Soc.*, **137**, 553–597, doi:10.1002/qj.828.

Ding, M., C. Xiao, Y. Li, J. Ren, S. Hou, B. Jin, and B. Sun, 2011: Spatial variability of surface mass balance along a traverse route from Zhongshan station to Dome A, Antarctica. *J. Glaciol.*, **57**, 658–666, doi:10.3189/002214311797409820.

Ebita, A., and Coauthors, 2011: The Japanese 55-year Reanalysis "JRA-55": An interim report. *SOLA*, **7**, 149–152, doi:10.2151/sola.2011-038.

ECMWF, 2008: IFS Documentation—CY33R1. Part IV: Physical processes. European Centre for Medium-Range Weather Forecasts, 162 pp. [Available online at http://www.ecmwf.int/en/elibrary/9227-part-iv-physical-processes.]

Ekaykin, A. A., 2003: Meteorological regime of central Antarctica and its role in the formation of isotope composition of snow thickness. Ph.D. thesis, Joseph Fourier University, 122 pp.

——, V. Y. Lipenkov, I. N. Kuz'mina, J. R. Petit, V. Masson-Delmotte, and S. J. Johnsen, 2004: The changes in isotope composition and accumulation of snow at Vostok Station over

the past 200 years. *Ann. Glaciol.*, **39**, 569–575, doi:10.3189/172756404781814348.

——, ——, and Y. A. Shibaev, 2012: Spatial distribution of the snow accumulation rate along the ice flow lines between Ridge B and Lake Vostok. *Led Sneg*, **4**, 123–128, doi:10.15356/2076-6734-2012-4-122-128.

Ettema, J., M. R. van den Broeke, E. van Meijgaard, and W. J. van de Berg, 2010: Climate of the Greenland ice sheet using a high-resolution climate model—Part 1: Evaluation. *Cryosphere*, **4**, 511–527, doi:10.5194/tc-4-511-2010.

Favier, V., and Coauthors, 2013: An updated and quality controlled surface mass balance dataset for Antarctica. *Cryosphere*, **7**, 583–597, doi:10.5194/tc-7-583-2013.

Fernandoy, F., H. Meyer, H. Oerter, F. Wilhelms, W. Graf, and J. Schwander, 2010: Temporal and spatial variation of stable isotope ratios and accumulation rates in the hinterland of Neumayer station, East Antarctica. *J. Glaciol.*, **56**, 673–687, doi:10.3189/002214310793146296.

Frezzotti, M., and Coauthors, 2004: New estimations of precipitation and surface sublimation in East Antarctica from snow accumulation measurements. *Climate Dyn.*, **23**, 803–813, doi:10.1007/s00382-004-0462-5.

——, and Coauthors, 2005: Spatial and temporal variability of snow accumulation in East Antarctica from traverse data. *J. Glaciol.*, **51**, 113–124, doi:10.3189/172756505781829502.

——, S. Urbini, M. Proposito, C. Scarchilli, and S. Gandolfi, 2007: Spatial and temporal variability of surface mass balance near Talos Dome, East Antarctica. *J. Geophys. Res.*, **112**, F02032, doi:10.1029/2006JF000638.

——, C. Scarchilli, S. Becagli, M. Proposito, and S. Urbini, 2013: A synthesis of the Antarctic surface mass balance during the last 800 yr. *Cryosphere*, **7**, 303–319, doi:10.5194/tc-7-303-2013.

Gallée, H., A. Trouvilliez, C. Agosta, C. Genthon, V. Favier, and F. Naaim-Bouvet, 2013a: Transport of snow by the wind: A comparison between observations in Adélie Land, Antarctica, and simulations made with the regional climate model MAR. *Bound.-Layer Meteor.*, **146**, 133–147, doi:10.1007/s10546-012-9764-z.

——, ——, C. Amory, C. Agosta, C. Genthon, X. Fettweis, V. Favier, and F. Naaim-Bouvet, 2013b: Simulations of blowing snow over Antarctica. *Proc. 2013 Int. Snow Science Workshop*, Grenoble, France, ISSP, 120–125.

Genthon, C., P. Lardeux, and G. Krinner, 2007: The surface accumulation and ablation of a coastal blue-ice area near Cap Prudhomme, Adélie Land, Antarctica. *J. Glaciol.*, **53**, 635–645, doi:10.3189/002214307784409333.

Goodwin, I. D., M. Higham, I. Allison, and J. Ren, 1994: Accumulation variability in eastern Kemp land, Antarctica. *Ann. Glaciol.*, **20**, 202–206.

Higham, M., and M. Craven, 1997: Surface mass balance and snow surface properties from the Lambert Glacier basin traverses 1990–94. Antarctic CRC Research Rep. 9, Cooperative Research Centre for the Antarctic and Southern Ocean Environment, 129 pp.

IPCC, 2013: *Climate Change 2013: The Physical Science Basis*. T. F. Stocker et al., Eds., Cambridge University Press, 1535 pp.

Jouzel, J., F. Vimeux, N. Caillon, G. Delaygue, G. Hoffmann, G. V. Masson-Delmotte, and F. Parrenin, 2003: Magnitude of isotope/temperature scaling for interpretation of central Antarctic ice cores. *J. Geophys. Res.*, **108**, 4361, doi:10.1029/2002JD002677.

Kaspari, S., P. A. Mayewski, D. A. Dixon, V. B. Spikes, S. B. Sneed, M. J. Handley, and G. S. Hamilton, 2004: Climate variability in West Antarctica derived from annual accumulation rate

records from ITASE firn/ice cores. *Ann. Glaciol.*, **39**, 585–594, doi:10.3189/172756404781814447.

Khodzher, T. V., L. P. Golobokova, E. Yu. Osipov, Yu. A. Shibaev, V. Ya. Lipenkov, O. P. Osipova, and J. R. Petit, 2014: Spatial–temporal dynamics of chemical composition of surface snow in East Antarctica along the Progress station–Vostok station transect. *Cryosphere*, **8**, 931–939, doi:10.5194/tc-8-931-2014.

Kobayashi, S., and Coauthors, 2015: The JRA-55 Reanalysis: General specifications and basic characteristics. *J. Meteor. Soc. Japan*, **93**, 5–48, doi:10.2151/jmsj.2015-001.

Krinner, G., O. Magand, I. Simmonds, C. Genthon, and J.-L. Dufresne, 2007: Simulated Antarctic precipitation and surface mass balance at the end of twentieth and twenty-first centuries. *Climate Dyn.*, **28**, 215–230, doi:10.1007/s00382-006-0177-x.

Kuipers Munneke, P., M. R. van den Broeke, J. T. M. Lenaerts, M. G. Flanner, A. S. Gardner, and W. J. van de Berg, 2011: A new albedo parameterization for use in climate models over the Antarctic ice sheet. *J. Geophys. Res.*, **116**, D05114, doi:10.1029/2010JD015113.

Laepple, T., M. Werner, and G. Lohmann, 2011: Synchronicity of Antarctic temperature and local solar insolation on orbital time scales. *Nature*, **471**, 91–94, doi:10.1038/nature09825.

Lazzara, M. A., L. M. Keller, T. Markle, and J. Gallagher, 2012: Fifty-year Amundsen–Scott South Pole station surface climatology. *Atmos. Res.*, **118**, 240–259, doi:10.1016/j.atmosres.2012.06.027.

Lenaerts, J. T. M., M. R. van den Broeke, S. J. Déry, G. König-Langlo, J. Ettema, and P. Kuipers Munneke, 2010: Modelling snowdrift sublimation on an Antarctic ice shelf. *Cryosphere*, **4**, 179–190, doi:10.5194/tc-4-179-2010.

——, ——, W. J. van de Berg, E. van Meijgaard, and P. Kuipers Munneke, 2012: A new, high-resolution surface mass balance map of Antarctica (1979–2010) based on regional atmospheric climate modeling. *Geophys. Res. Lett.*, **39**, L04501, doi:10.1029/2011GL050713.

Lenderink, G., E. van den Hurk, A. van Meijgaard, A. P. van Ulden, and H. Cuijpers, 2003: Simulation of present-day climate in RACMO2: First results and model developments. KNMI Tech. Rep. 252, 24 pp.

Ligtenberg, S. R. M., W. J. van de Berg, M. R. van den Broeke, J. G. L. Rae, and E. van Meijgaard, 2013: Future surface mass balance of the Antarctic ice sheet and its influence on sea level change, simulated by a regional atmospheric climate model. *Climate Dyn.*, **41**, 867–884, doi:10.1007/s00382-013-1749-1.

——, J. T. M. Lenaerts, M. R. van den Broeke, and T. A. Scambos, 2014: On the formation of blue ice on Byrd Glacier, Antarctica. *J. Glaciol.*, **60**, 41–50, doi:10.3189/2014JoG13J116.

Magand, O., C. Genthon, M. Fily, G. Krinner, G. Picard, M. Frezzotti, and A. A. Ekaykin, 2007: An up-to-date quality-controlled surface mass balance data set for the 90°–180°E Antarctica sector and 1950–2005 period. *J. Geophys. Res.*, **112**, D12106, doi:10.1029/2006JD007691.

Mayewski, P. A., and D. A. Dixon, 2013: U.S. International Trans Antarctic Scientific Expedition (US ITASE) glaciochemical data, version 2. National Snow and Ice Data Center, accessed 5 January 2015, doi:10.7265/N51V5BXR.

Medley, B., and Coauthors, 2013: Airborne-radar and ice-core observations of annual snow accumulation over Thwaites Glacier, West Antarctica confirm the spatiotemporal variability of global and regional atmospheric models. *Geophys. Res. Lett.*, **40**, 3649–3654, doi:10.1002/grl.50706.

Monaghan, A. J., and Coauthors, 2006a: Insignificant change in Antarctic snowfall since the international geophysical year. *Science*, **313**, 827–831, doi:10.1126/science.1128243.

——, D. H. Bromwich, and S.-H. Wang, 2006b: Recent trends in Antarctic snow accumulation from Polar MM5 simulations. *Philos. Trans. Roy. Soc. London*, **364**, 1683–1708, doi:10.1098/rsta.2006.1795.

Oerter, H., F. Wilhelms, F. Jung-Rothenhäusler, F. Göktas, H. Miller, W. Graf, and S. Sommer, 2000: Accumulation rates in Dronning Maud Land, Antarctica, as revealed by dielectric-profiling measurements of shallow firn cores. *Ann. Glaciol.*, **30**, 27–34, doi:10.3189/172756400781820705.

Richardson, C., E. Aarholt, S. E. Hamran, P. Holmlund, and E. Isaksson, 1997: Spatial distribution of snow in western Dronning Maud Land, East Antarctica, mapped by a ground-based snow radar. *J. Geophys. Res.*, **102**, 20 343–20 353, doi:10.1029/97JB01441.

Rienecker, M. R., and Coauthors, 2011: MERRA: NASA's Modern-Era Retrospective Analysis for Research and Applications. *J. Climate*, **24**, 3624–3648, doi:10.1175/JCLI-D-11-00015.1.

Rignot, E., I. Velicogna, M. R. van den Broeke, A. Monaghan, and J. T. M. Lenaerts, 2011: Acceleration of the contribution of the Greenland and Antarctic ice sheets to sea level rise. *Geophys. Res. Lett.*, **38**, L05503, doi:10.1029/2011GL046583.

Saha, S., and Coauthors, 2010: The NCEP Climate Forecast System Reanalysis. *Bull. Amer. Meteor. Soc.*, **91**, 1015–1057, doi:10.1175/2010BAMS3001.1.

Scambos, T. A., and Coauthors, 2012: Extent of low-accumulation 'wind glaze' areas on the East Antarctic plateau: Implications for continental ice mass balance. *J. Glaciol.*, **58**, 633–647, doi:10.3189/2012JoG11J232.

Scarchilli, C., M. Frezzotti, P. Grigioni, L. De Silvestri, L. Agnoletto, and S. Dolci, 2010: Extraordinary blowing snow transport events in East Antarctica. *Climate Dyn.*, **34**, 1195–1206, doi:10.1007/s00382-009-0601-0.

Schlosser, E., 1999: Effects of seasonal variability of accumulation on yearly mean δ^{18}O values in Antarctic snow. *J. Glaciol.*, **45**, 463–468.

——, H. Anschütz, E. Isaksson, T. Martma, D. Divine, and O.-A. Nøst, 2012: 2012: Surface mass balance and stable oxygen isotope ratios from shallow firn cores on Fimbulisen, East Antarctica. *Ann. Glaciol.*, **53**, 70–78, doi:10.3189/2012AoG60A102.

——, ——, D. Divine, T. Martma, A. Sinisalo, S. Altnau, and E. Isaksson, 2014: Recent climate tendencies on an East Antarctic ice shelf inferred from a shallow firn core network. *J. Geophys. Res. Atmos.*, **119**, 6549–6562, doi:10.1002/2013JD020818.

Shepherd, A., and Coauthors, 2012: A reconciled estimate of ice-sheet mass balance. *Science*, **338**, 1183–1189, doi:10.1126/science.1228102.

Siegert, M. J., R. C. A. Hindmarsh, and G. S. Hamilton, 2003: Evidence of a large surface ablation zone in central East Antarctica during the last Ice Age. *Quat. Res.*, **59**, 114–121, doi:10.1016/S0033-5894(02)00014-5.

Sinisalo, A., and Coauthors, 2013: Surface mass balance on Fimbul ice shelf, East Antarctica: Comparison of field measurements and large-scale studies. *J. Geophys. Res. Atmos.*, **118**, 11 625–11 635, doi:10.1002/jgrd.50875.

Stenni, B., M. Proposito, R. Gragnani, O. Flora, J. Jouzel, S. Falourd, and M. Frezzotti, 2002: Eight centuries of volcanic signal and climate change at Talos Dome (East Antarctica). *J. Geophys. Res.*, **107**, 4076, doi:10.1029/2000JD000317.

Thomas, E. R., G. J. Marshall, and J. R. McConnell, 2008: A doubling in snow accumulation in the western Antarctic Peninsula since 1850. *Geophys. Res. Lett.*, **35**, L01706, doi:10.1029/2007GL032529.

——, J. S. Hosking, R. R. Tuckwell, R. A. Warren, and E. C. Ludlow, 2015: Twentieth century increase in snowfall in coastal West Antarctica. *Geophys. Res. Lett.*, **42**, 9387–9393, doi:10.1002/2015GL065750.

Thompson, L. G., D. A. Peel, E. Mosley-Thompson, R. Mulvaney, J. Dai, P. N. Lin, M. E. Davis, and C. F. Raymond, 1994: Climate change since AD 1510 on Dyer Plateau, Antarctic Peninsula: Evidence for recent climate change. *Ann. Glaciol.*, **20**, 420–426.

van de Berg, W. J., and B. Medley, 2016: Upper air relaxation in RACMO2 significantly improves modelled interannual surface mass balance variability in Antarctica. *Cryosphere*, **10**, 459–463, doi:10.5194/tc-10-459-2016.

——, M. R. van den Broeke, C. H. Reijmer, and E. van Meijgaard, 2005: Characteristics of the Antarctic surface mass balance, 1958–2002, using a regional atmospheric climate model. *Ann. Glaciol.*, **41**, 97–104, doi:10.3189/172756405781813302.

——, ——, C. Reijmer, and E. Van Meijgaard, 2006: Reassessment of the Antarctic surface mass balance using calibrated output of a regional atmospheric climate model. *J. Geophys. Res.*, **111**, D11104, doi:10.1029/2005JD006495.

Van Lipzig, N. P. M., and M. R. van den Broeke, 2002: A model study on the relation between atmospheric boundary-layer dynamics and poleward atmospheric moisture transport in Antarctica. *Tellus*, **54A**, 497–511, doi:10.1034/j.1600-0870.2002.201404.x.

van Ommen, T. D., and V. Morgan, 2010: Snowfall increase in coastal East Antarctica linked with southwest Western Australian drought. *Nat. Geosci.*, **3**, 267–272, doi:10.1038/ngeo761.

van Wessem, J. M., and Coauthors, 2014a: Improved representation of East Antarctic surface mass balance in a regional atmospheric climate model. *J. Glaciol.*, **60**, 761–770, doi:10.3189/2014JoG14J051.

——, C. H. Reijmer, J. T. M. Lenaerts, W. J. Van de Berg, M. R. Van den Broeke, and E. Van Meijgaard, 2014b: Updated cloud physics in a regional atmospheric climate model improves the modelled surface energy balance of Antarctica. *Cryosphere*, **8**, 125–135, doi:10.5194/tc-8-125-2014.

Vaughan, D. G., J. L. Bamber, M. Giovinetto, J. Russell, and A. P. R. Cooper, 1999: Reassessment of net surface mass balance in Antarctica. *J. Climate*, **12**, 933–946, doi:10.1175/1520-0442(1999)012<0933:RONSMB>2.0.CO;2.

Velicogna, I., and J. Wahr, 2006: Measurements of time-variable gravity show mass loss in Antarctica. *Science*, **311**, 1754–1756, doi:10.1126/science.1123785.

Wang, Y., S. Hou, W. Sun, J. T. M. Lenaerts, M. R. van den Broeke, and J. M. van Wessem, 2015: Recent surface mass balance from Syowa Station to Dome F, East Antarctica: Comparison of field observations, atmospheric reanalyses, and a regional atmospheric climate model. *Climate Dyn.*, **45**, 2885–2899, doi:10.1007/s00382-015-2512-6.

Wen, J., J. Kang, D. Wang, B. Sun, Y. Li, Z. Li, and J. Li, 2001: Density, stratigraphy and accumulation at DT001 in Princess Elizabeth Land, East Antarctic Ice Sheet. *Polar Meteor. Glaciol.*, **15**, 43–54.

Wouters, B., J. L. Bamber, M. R. van den Broeke, J. T. M. Lenaerts, and I. Sasgen, 2013: Limits in detecting acceleration of ice sheet mass loss due to climate variability. *Nat. Geosci.*, **6**, 613–616, doi:10.1038/ngeo1874.

Xiao, C., J. Ren, D. H. Qin, Z. Q. Li, W. Z. Sun, and I. Allison, 2001: Complexity of the climatic regime over the Lambert Glacier basin of the East Antarctica ice sheet: Firn core evidences. *J. Glaciol.*, **47**, 160–163, doi:10.3189/172756501781832539.

Zwally, H. J., and M. B. Giovinetto, 2011: Overview and assessment of Antarctic Ice-Sheet mass balance estimates: 1992–2009. *Surv. Geophys.*, **32**, 351–376, doi:10.1007/s10712-011-9123-5.